Calculating the water and heat balances of the Eastern Mediterranean Basin using ocean modelling and available meteorological, hydrological and ocean data

Mohamed Shaltout[1*]
Anders Omstedt[2]

[1] Faculty of Science,
Department of Oceanography,
University of Alexandria,
Alexandria, Egypt;

currently:

Department of Earth Sciences,
University of Gothenburg,
P.O. Box 460, Götenburg 40530, Sweden;

e-mail: mohamed.shaltout@gvc.gu.se

*corresponding author

[2] Department of Earth Sciences,
University of Gothenburg,
P.O. Box 460, Götenburg 40530, Sweden

Abstract

Eastern Mediterranean water and heat balances were analysed over 52 years. The modelling uses a process-oriented approach resolving the one-dimensional equations of momentum, heat and salt conservation; turbulence is modelled using a two-equation model. The results indicate that calculated temperature and salinity follow the reanalysed data well. The water balance in the Eastern Mediterranean basin was controlled by the difference between inflows and outflows through the Sicily Channel and by net precipitation. The freshwater component displayed

The complete text of the paper is available at http://www.iopan.gda.pl/oceanologia/

a negative trend over the study period, indicating increasing salinity in the basin. The heat balance was controlled by heat loss from the water surface, solar radiation into the sea and heat flow through the Sicily Channel. Both solar radiation and net heat loss displayed increasing trends, probably due to decreased total cloud cover. In addition, the heat balance indicated a net import of approximately 9 W m^{-2} of heat to the Eastern Mediterranean Basin from the Western Basin.

1. Introduction

New initiatives are being taken in the Mediterranean region, where climate change may pose a severe threat. In the Hydrological cycle in the Mediterranean Experiment (HyMex) programme (http://www.hymex.org/), the water cycle is of major concern. To support this initiative, we will adapt the knowledge gained from the Baltic Sea Experiment (BALTEX) programme to make it applicable to the Mediterranean region. This paper is the first such attempt and addresses the water and heat balances of the Eastern Mediterranean Basin (EMB). The approach follows that of Omstedt & Nohr (2004), who used a process-based ocean model together with available meteorological, hydrological and in situ ocean data to analyse the water and heat cycles of the Baltic Sea.

The Eastern Mediterranean Basin (EMB), which extends from 11°E to 36°E and from 30°N to 46°N, is a semi-enclosed basin with a negative water balance (i.e. evaporation greater than precipitation plus river runoff). The Sicily Channel (149 km wide) and Strait of Messina (4 km wide) connect the Eastern and Western Mediterranean Sea basins (Figure 1). The Bosphorus-Marmara-Dardanelles system connects the Black Sea with the EMB. The exchange through the Strait of Messina is much smaller than that through
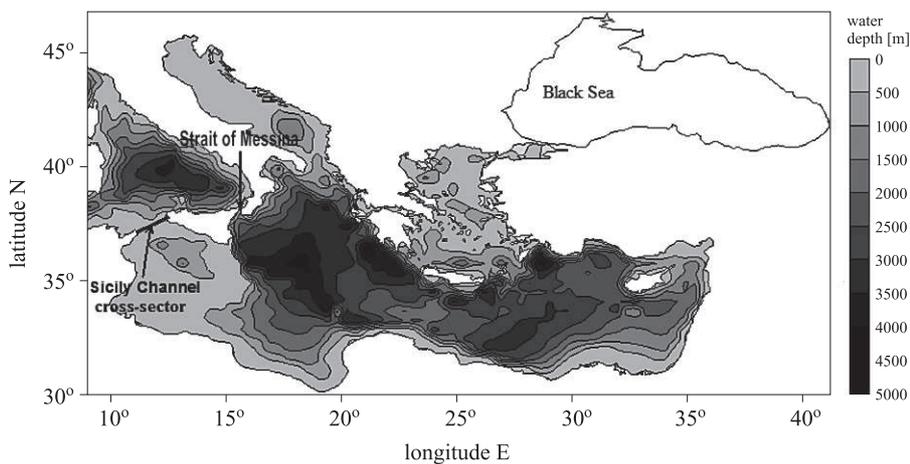

Figure 1. Bathymetric chart of the Eastern Mediterranean Basin

the Sicily Channel and is therefore neglected. The present study will treat the Black Sea solely as river runoff with a salinity 18 PSU lower than that of the Mediterranean. The EMB will be regarded as a single natural basin with in- and outflows, and processes such as air-sea interaction, land-sea interaction (i.e. river runoff), diapycnal mixing, overturning circulation (i.e. Atlantic water inflows, intermediate and deep water formation), exchange through the Sicily Channel and brackish water outflow from the Black Sea will be emphasized. The River Nile and Black Sea play important roles in changing the freshwater content of the EMB. The model will be driven by available meteorological and hydrological data and validated using available oceanographic observations. Based on the calculations, conclusions will be drawn regarding the water (salinity) and heat (temperature) balances.

The thermohaline water structure in the Eastern Mediterranean is an important climatic issue, as its changes may affect marine systems through changes in deep water formation, current systems and sea level variations. Freshwater input to the EMB mixes with sea surface water and surface water flows from the Western Mediterranean Basin through the Sicily Channel. The outflow of water over the Sicily Channel sill (Figure 2b, page 205) is responsible for water loss from the EMB. The negative value of net precipitation (precipitation P minus evaporation E) influences the salinity balance. In the winter, because of evaporation and heat loss, the Levantine surface water may become dense enough to form Levantine intermediate-depth water (200–500 m) or Levantine deep water. However, deep water forms only occasionally. Roether & Schlitzer (1991) demonstrated that the average deep water formation rate in the EMB is approximately 0.3×10^6 m^3 s^{-1}. Malanotte-Rizzoli et al. (1999) found that deep water formation takes place in the Adriatic, Aegean and Levantine sub-basins. Zervakis et al. (2000) demonstrated that the enhanced negative water balance of the Eastern Mediterranean leads to a new source of deep water formation, especially in the Aegean Sea.

Béranger et al. (2002) investigated the mean inflow to the EMB through the Sicily Channel using numerical modelling. They estimated that the mean inflow through the Channel was approximately $1.05 \pm 0.35 \times 10^6$ m^3 s^{-1} over a 13-year period. Stansfield et al. (2002) estimated the surface flow to the Eastern basin using observations from conductivity-temperature-depth (CTD) data. They found a surface flow of Atlantic water (AW) origin flowing through the Sicily Channel above a depth of 150 m. The outflow of Levantine intermediate water (LIW) through the Sicily Channel occurred in deeper layers. Sorgente et al. (2003) used the Princeton Ocean Model (POM) to study the flow through the Sicily Channel. This modelling identified two main AW veins, one in the south along the African coast

and the other in the north along the Sicilian coast. Based on geostrophic calculations using CTD data from April 2003–October 2003, Ferjani & Gana (2010) indicated that the mean inflow and outflow through the western side of the Sicily Channel were 0.5 and 0.4×10^6 m^3 s^{-1} respectively. Stanev et al. (2000) characterized the water exchange through the Bosphorus-Marmara-Dardanelles system as a two-layer flow, in which Black Sea water occupied the surface layer (average flow of 0.019×10^6 m^3 s^{-1}) and Mediterranean water occupied the deep layer (average flow of 0.009×10^6 m^3 s^{-1}). Recent estimates indicate a reduction in inflow of approximately 0.003×10^6 m^3 s^{-1}, which affects the North Aegean Sea circulation (Stanev & Peneva 2002). Nixon (2003) and Ludwig et al. (2009) estimated that the average discharge of the River Nile to the Mediterranean basin after the construction of the Aswan High Dam decreased by a factor of more than two.

The paper aims to: (1) examine the water exchange through the Sicily Channel, (2) calculate the long-term change in vertical temperature and salinity distribution in the Eastern Mediterranean Basin, and (3) examine the heat and water balances of the Eastern Mediterranean Basin. The study uses a simple ocean model to analyse a large set of meteorological and hydrological data used for forcing. The model simulations are validated and the main conclusions are drawn using independent oceanographic observations. The paper is structured as follows: section 2 presents the data and models used; section 3 presents the results, while section 4 discusses them; finally, the appendices provide a full description of the model.

2. Material and methods

2.1. Data sources

The study relies on the numerical modelling of the heat and water balances of the Eastern Mediterranean Basin and the water exchange through the Sicily Channel. The present version of the model is vertically resolved and time-dependent, based on horizontally-averaged input data over the study area and with in- and outflows controlling the vertical circulation. The meteorological data were horizontally averaged using linear interpolation over the EMB to describe the general features of the forcing data. Exchange through the Sicily Channel was modelled using: (1) current speeds across the Sicily Channel calculated from satellite recordings, (2) evaporation rates calculated from the model, (3) observed precipitation rates, and (4) observed river data. The period studied was 1958–2009. Several data sources have been used in this study, as follows:

1. Mediterranean Sea absolute dynamic topography data from May 2006 to October 2009. These data were extracted from the Archiving, Validation and Interpretation of Satellite Oceanographic data (AVISO) database available at http://www.aviso.oceanobs.com/en/home/index.html. The absolute dynamic topography was calculated as the sum of the sea level anomaly and mean dynamic topography. The data were calculated using a 1-day temporal scale and $1/3°$ spatial scale and used to study exchange through the Sicily Channel.

2. Digitized bathymetric data obtained from the British Oceanographic Data Centre with a 0.5-min grid (http://www.bodc.ac.uk/data/online_delivery/gebco/). These data were used when calculating the cross-sectional area of the Sicily Channel and the areadepth distribution of the EMB.

3. Data on river runoff into the EMB and Black Sea covering the 1976–1987 period obtained from the Center for Sustainability and the Global Environment (SAGE) and available at www.sage.wisc.edu, together with the Ludwig et al. (2009) river database covering the 1958–2000 period, were used as forcing for the model simulations.

4. Data on sea surface temperature, air temperature at a height of 2 m [°C], horizontal wind components at a height of 10 m [m s^{-1}], percentage of total cloud cover, precipitation and relative humidity for the EMB were extracted from the European Centre for Medium-Range Weather Forecasts (ECMWF) data server for meteorological data with a 6-h temporal resolution. These data have a spatial resolution of $2.5° \times 2.5°$ and $1.5° \times 1.5°$ over the 1958–1988 and 1989–2009 periods respectively.

5. Data on evaporation rates for EBM over the 1958–2009 period extracted at 6-h intervals with a $2.5° \times 2.5°$ spatial resolution were obtained using the National Center for Environmental Prediction's (NCEP) meteorological database (http://www.esrl.noaa.gov/psd/data/) and used in the validation study only.

6. Two datasets were used to validate the model results: the Mediterranean Data Archaeology (MEDAR) annual temperature and salinity reanalysed database (Rixen et al. 2005) with a $0.2°$ resolution from 1958 to 2002 and vertical resolutions of 0, 5, 10, 20, 30, 50, 75, 100, 125, 150, 200, 250, 300, 400, 500, 600, 800, 1000, 1200, 1500, 2000, 2500, 3000 and 4000 m; reanalysed temperature (1958–2008) and salinity (1958–1998) data for the EMB taken at one-month intervals with a spatial distribution of $1° \times 1°$, obtained from the National Oceanographic Data Center (NODC, http://www.nodc.noaa.gov).

2.2. Volume and salt conservation

Starting from the volume conservation principle, we can formulate the water balance equation as follows:

$$A_s \frac{\partial \eta}{\partial t} = Q_{in} - Q_{out} + A_s(P - E) + Q_f, \tag{1}$$

where A_s is the Eastern Mediterranean surface area, $\frac{\partial \eta}{\partial t}$ the change in sea level with time and Q_f the river discharge to the basin, calculated as the sum of total river runoff to the EMB and the Black Sea brackish water. In the present application, we assume that the volume fluxes related to surface elevation changes are small relative to the other contributions, which means that the left-hand side of equation (1) is close to zero, which is valid for long-term scales.

2.3. Heat balance

From conservation principles, we can formulate the heat balance equation for a semi-enclosed sea area, as follows (e.g. Omstedt 2011):

$$\frac{dH}{dt} = (F_i - F_o - F_{\text{loss}})A_s, \tag{2}$$

where $H = \int \int \rho c_p T \, dz \, dA$ is the total heat content of the EMB, F_{in} and F_{out} the heat fluxes associated with in- and outflows through the Sicily Channel respectively (calculated according to $F_{in} = \rho c_p T_{in} Q_{in}$ and $F_{out} = \rho c_p T_{out} Q_{out}$ respectively), T_{in} and T_{out} the respective temperatures of the in- and outflowing surface water from the Western Mediterranean Basin, c_p the heat capacity and F_{loss} the total heat loss to the atmosphere (the fluxes are positive when going from the water to the atmosphere). F_{loss} is formulated as follows:

$$F_{\text{loss}} = F_n + F_s^w, \tag{3}$$

where

$$F_n = F_h + F_e + F_l + F_{prec}. \tag{4}$$

The various terms in equations (3) and (4) stand for the following: F_h is the sensible heat flux, F_e the latent heat flux, F_l the net long-wave radiation, and F_s^w the solar radiation to the water surface. The various heat flux components are presented in greater detail in Appendix A2.

2.4. Water exchange through the Sicily Channel

To calculate the heat and water balances of the EMB, the water exchanges through the Sicily Channel are needed. These exchanges are approximated as a two-layer exchange flow, including a surface inflow (Q_{in})

from the Western Mediterranean Basin and a deeper outflow (Q_{out}) from the Eastern to Western basins over the Sicily Channel sill. To calculate the surface inflow, satellite sea level data (η) across the Channel were used, assuming geostrophic flows:

$$U_g = \frac{-g}{f}\frac{\partial \eta}{\partial y}, \quad V_g = \frac{g}{f}\frac{\partial \eta}{\partial x} \quad \text{and} \quad W_g^2 = U_g^2 + V_g^2,$$

where f is the Coriolis parameter, g the gravity force, U_g and V_g the velocity components in the x and y directions respectively, and W_g the surface geostrophic speed. For simplification, we assumed that the depth of the surface layer was 150 m (see e.g. Stansfield et al. 2002). Moreover, a fixed depth of the surface layer (150 m) is acceptable in view of the very small cross-sectional area of the channel between 100 to 150 m depth compared with the cross-sectional area between the surface and 100 m depth (Figure 2b).
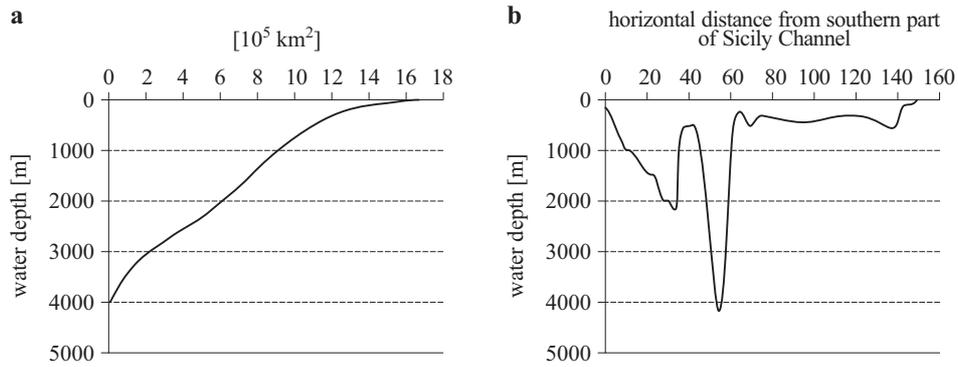
Figure 2. a) Aarea-depth distribution in the Eastern Mediterranean Basin, b) vertical bathymetric cross section across the Sicily Channel (see Figure 1, page 200)

The surface flow from the Western to the Eastern Mediterranean basins (Q_{in}) was calculated by dividing the horizontal distance from the northern to southern Sicily Channel into cross-sectional sectors:

$$Q_{in} = \sum_{i=1}^{17}\sum_{j=1}^{3} Wn_{i,j}A_{i,j}, \tag{5}$$

where W_n is the normal cross-channel component of the geostrophic flow, A the corresponding cross-sectional area (Figure 1), and i and j the respective indexes for the horizontal and vertical cross-sections, assuming three 50-m-thick vertical homogeneous layers distributed according to the bathymetric cross-section in the Sicily Channel (Figure 2b).

From water volume conservation in the EMB (equation (1)), the deeper flows were then calculated using climatological oceanographic data.

2.5. Model, forcing, and lateral boundary conditions

The model simulated the properties of the EMB based on horizontally averaged advective-diffusive conservation equations for volume, heat, momentum, and salinity, including a two-equation turbulent model. The Program for Boundary Layers in the Environment (PROBE) equation solver, documented and available in Omstedt (2011), was used; the present application for the EMB is called PROBE-EMB and the equations are fully described in Appendix A1. The model used the area-depth distribution of the Eastern Mediterranean Basin and was forced using meteorological and river runoff data. EMB water and heat cycles were simulated by running the PROBE-EMB model from 1958 to 2009 with a 600-s temporal resolution and a vertically resolved grid with 190 grid cells, expanding from surface to bottom.

Satellite sea level observations across the Sicily Channel and surface temperature and salinity on the western side of the Channel were used as lateral boundary conditions. Meteorological data, comprising surface air temperature [°C], zonal and meridional wind speed [m s^{-1}], total cloud cover percentage, relative humidity and precipitation rate [m s^{-1}], were used as forcing data. Air temperature data were corrected for land influence by comparing them with sea surface temperatures. River runoff data were calculated from available data as monthly means. The most important river discharges into the EMB at present are from the P_o (1583.1 m^3 s^{-1}), Adige (203.2 m^3 s^{-1}), Drin (219.4 m^3 s^{-1}), Vjose (145.8 m^3 s^{-1}), Shkumbini (35.7 m^3 s^{-1}), Marista (111.4 m^3 s^{-1}), Buyuk Menderes (98.5 m^3 s^{-1}), Ceyhan (222.5 m^3 s^{-1}) and Nile (2275.5 and 1245.4 m^3 s^{-1}, before and after 1964 respectively). The annual averaged river runoff values are 5000 and 3850 m^3 s^{-1}, before and after 1964 respectively, the change being due to the building of the Aswan High Dam. The Black Sea is modelled as river runoff but with a salinity 18 PSU lower than that of the EMB. The most significant rivers flowing into the Black Sea are the Danube (6766 m^3 s^{-1}), Dnieper (1506 m^3 s^{-1}), Rioni (408 m^3 s^{-1}), Dniester (375 m^3 s^{-1}), Kizilirmak (202 m^3 s^{-1}), Sakarya (193 m^3 s^{-1}) and southern Bug (110 m^3 s^{-1}). The average annual Black Sea discharge into the EMB is 7212.9 m^3 s^{-1}.

To represent the southern Tyrrhenian Basin, lateral boundary parameters for surface salinity and water temperature were applied. Surface salinity was calculated as monthly means using data obtained from the National Oceanographic Data Center. Surface temperature was calculated using the European Centre for Medium-Range Weather Forecasts database

with a 6-h temporal resolution. The monthly average southern Tyrrhenian surface temperature and salinity were 13.4–28.5°C and 37.15–38.07 PSU respectively over the study period.

Equation (5) was applied in calculating daily Q_{in} values from May 2006 to June 2009 using the AVISO satellite database. These values were then used for the whole period studied; although this represents an approximation, it is supported as tides are mainly short-term and periodic and the differences between the monthly average values of surface temperature and salinity for the eastern and western sides of the Sicily Channel are small. In future work, the Mediterranean climate system will be modelled using a large number of coupled sub-basin models, with the Sicily Channel flow being treated as a baroclinic exchange flow. The sensitivity of the assumption will be further analysed by running several sensitivity experiments (see section 3.2).

Bathymetric information and the area-depth distribution of the studied basin are depicted in Figures 1 and 2. The surface area is 1.67×10^{12} m^2, the water volume 2.4×10^{15} m^3, the average depth 1430 m and the maximum depth 5097 m. The annual average freshwater runoff was 12 943 m^3 s^{-1}, and the average precipitation and evaporation were 1.58 and 3.76 mm day^{-1} respectively. Moreover, the average monthly surface salinity and water temperature over the entire basin ranged from 38.3 to 38.8 PSU and 14.8 to 27°C respectively. The cross-sectional area of the Sicily Channel was calculated from bathymetric data (Figure 2b). Figure 2b shows that the Channel width from the southern to the northern parts is approximately 149 km and that the southern part is deeper than the northern part. The maximum depth across the Channel is 830 m.

3. Results

3.1. Water exchange through the Sicily Channel

Satellite data on the sea level across the Sicily Channel were used to calculate the surface current flow from the western to eastern basins using equation (5). Figure 3 depicts some examples from these calculations of how the surface currents can take various routes. These routes must be considered when measuring or calculating the Channel exchange. To resolve the mesoscale currents passing through the channel, the area was divided into 17 grid cells from which the Q_{in} values were calculated.

The temporal variations in the surface- and deep-layer flows are shown in Figure 4. The calculated surface flows over the period (early June 2006– late June 2009) ranged from 0.25 to 2.56×10^6 m^3 s^{-1}, averaging $1.16 \pm 0.34 \times 10^6$ m^3 s^{-1}, while the deep flows were in the same range but with
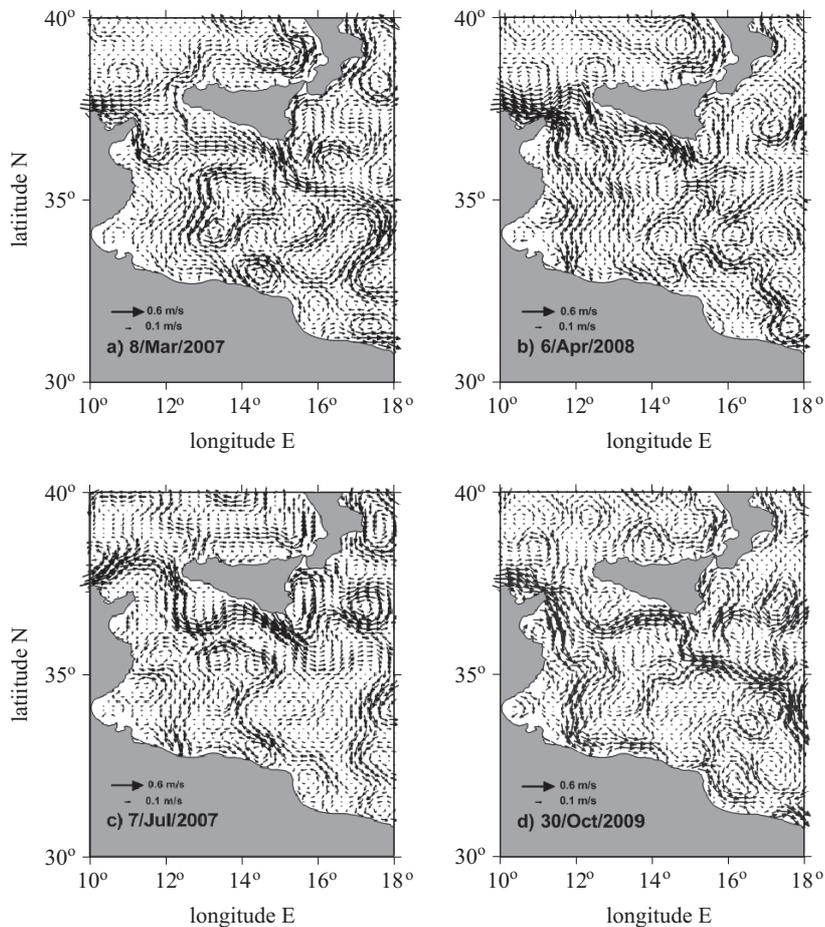
Figure 3. Calculated surface geostrophic current speeds near the Sicily Channel on four dates (arrow length increases linearly with increasing current speed). These dates were selected to illustrate the most important transport systems from the Western to Eastern basins

a slightly lower averaged value of $1.13 \pm 0.36 \times 10^6$ m^3 s^{-1}, indicating a loss of water in the EMB due to evaporation.

3.2. Model validation and sensitivity

The PROBE-EMB model results were first examined by comparing modelled and reanalysed monthly surface temperatures and salinities (i.e. the MEDAR and NODC datasets), and the results are illustrated in Figure 5. The modelled seasonal and interannual variations in the surface temperatures and salinities realistically follow the observations. However, the observations indicate periods of high surface salinity that
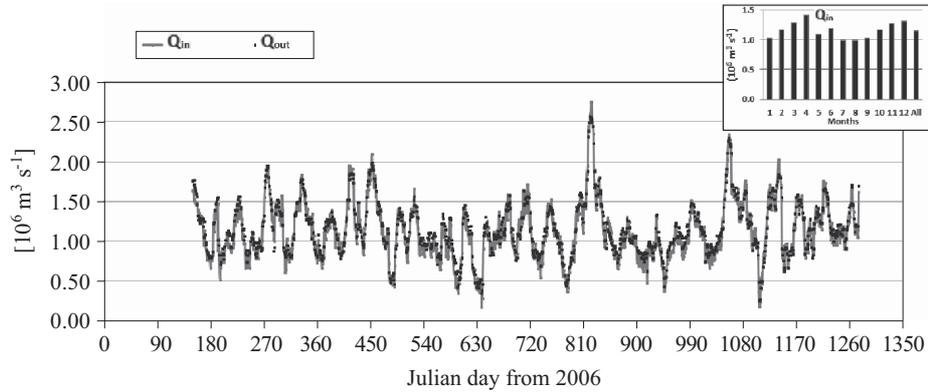
Figure 4. Time series of average surface flow (Q_{in}) and deep outflow (Q_{out}) through the Sicily Channel. The monthly average Q_{in} is shown in the upper right corner
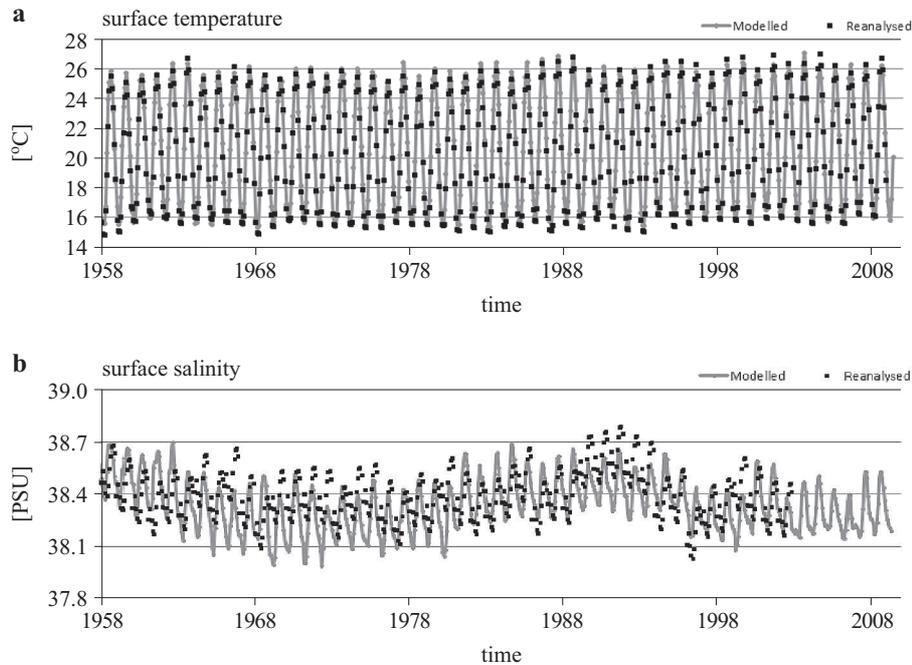
Figure 5. Surface modelled and reanalysed a) temperatures and b) salinities in the Eastern Mediterranean Basin

are underestimated by the model. Yearly averaged temperatures and salinities for the surface (0–150 m), intermediate (150–600 m) and deep (below 600 m) layers are presented in Figure 6. The modelled surface temperature follows the reanalysed temperature closely with a correlation
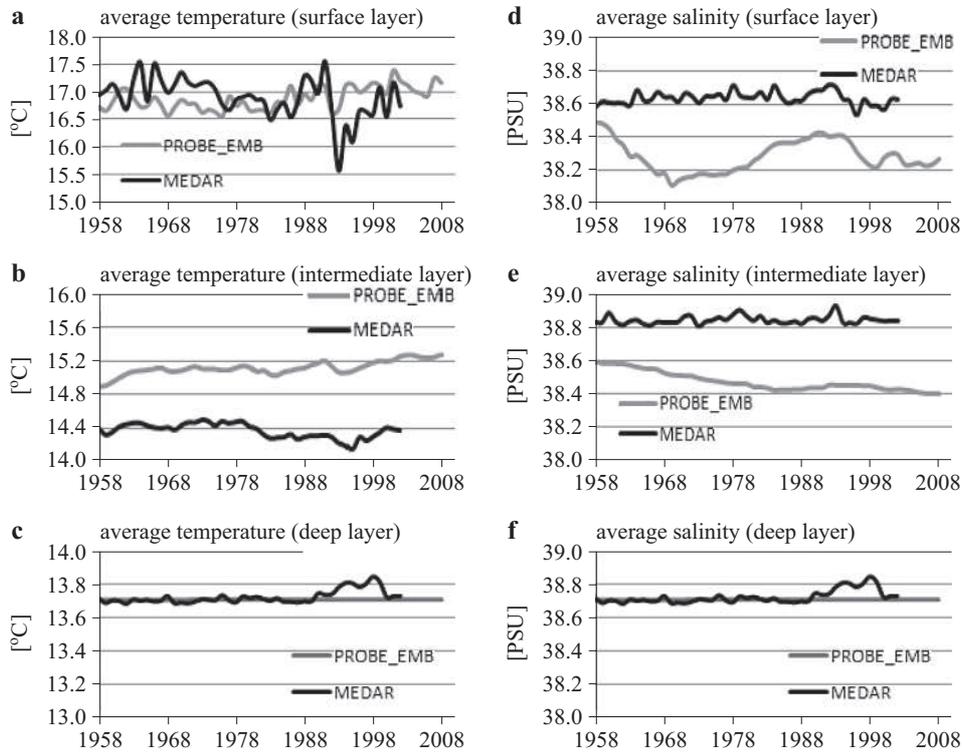
Figure 6. Yearly average temperatures and salinities of different layers of the Eastern Mediterranean Basin: surface layer (0–150 m depth), intermediate-depth layer (150–600 m depth) and deep layer (below 600 m depth)

(R) of 0.98 and a standard error of 0.7°C. The mean modelled and reanalysed surface temperatures over the study period were calculated to be 20.65 ± 3.7 and 20.3 ± 3.7°C respectively. Average modelled and reanalysed surface salinities were calculated to be 38.34 ± 0.14 and 38.39 ± 0.14 PSU respectively, with a correlation of 0.6 and a standard error of 0.11 PSU. In the intermediate layer, the yearly simulated temperate and salinity are over- and underestimated by 0.7°C and -0.37 PSU respectively, indicating that local processes such as deep-water convection need to be considered. Moreover, the MEDAR data set shows an insignificant trend of intermediate layer salinity content, while our model results indicate a small negative trend. This could be explained by the horizontal averaging for the whole EMB, which leads to reduced deep water formation. However, there is only a negligible bias between the simulated and calculated deep layer temperatures/salinities.

To investigate the heat balance in some detail, PROBE-EMB modelled evaporation rates were compared with meteorological modelled evaporation
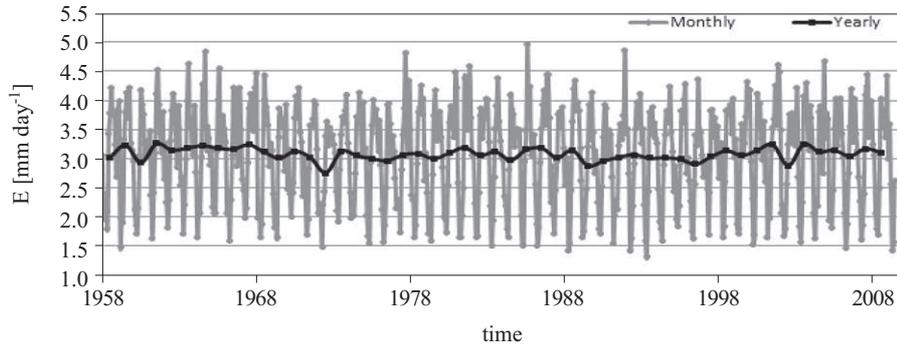
Figure 7. Modelled monthly and yearly average evaporation (E) rates for the Eastern Mediterranean Basin
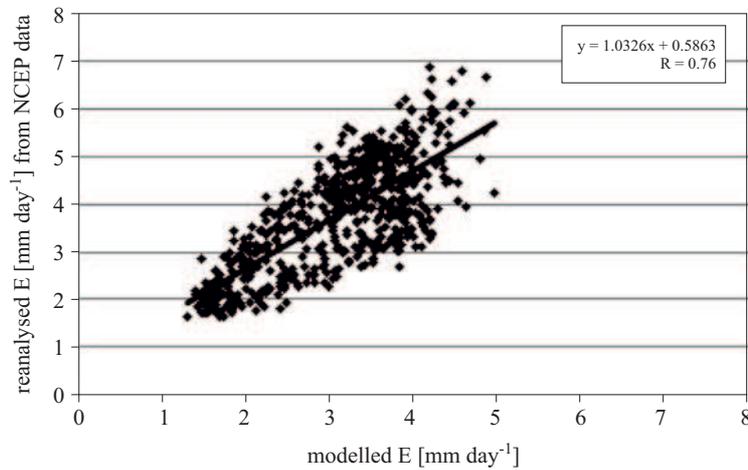
Figure 8. Monthly scatter plot of the evaporation rates calculated from the present ocean model and from the NCEP reanalysed evaporation rates for the Eastern Mediterranean Basin

data. This is an important test of the forcing fields and the modelling, as the evaporation rates were calculated independently using both methods. For the meteorological data, we used the NCEP reanalysed data, an independent dataset. Figure 7 depicts the monthly and yearly average values of modelled evaporation rates based on the PROBE-EMB simulations. Figure 8 depicts the scatterplot of modelled and NCEP reanalysed evaporation rates for the EMB. Over the study period, modelled evaporation rates ranged from 0.2 to 1.3 mm day^{-1}, with an average of 3.1 ± 1.5 mm day^{-1}. The monthly average evaporation rates over the study period ranged from 4.95 ± 1.8 mm day^{-1} in August 1985 to 1.31 ± 0.45 mm day^{-1} in May 1993, while the yearly average

evaporation rates ranged from 3.26 mm day^{-1} in 1961 to 2.74 mm day^{-1} in 1972. The reanalysed and modelled monthly evaporation rates agreed fairly well, with a correlation of 0.76 and a standard error of 0.5 mm day^{-1}.

The PROBE-EMB model results for surface temperature, salinity and evaporation rates were also calculated as monthly means (Figure 9): the monthly average surface temperature ranged from $15.8 \pm 0.32°$C in March to $25.98 \pm 0.44°$C in August; the monthly average surface salinity ranged from 38.19 ± 0.09 PSU in May to 38.5 ± 0.09 PSU in September; and the monthly average evaporation rates over the study period ranged from 1.78 ± 0.78 mm day^{-1} in April to 3.91 ± 1.08 mm day^{-1} in August. In the summer, surface temperature and evaporation reached their maximum values, as did surface salinity values.
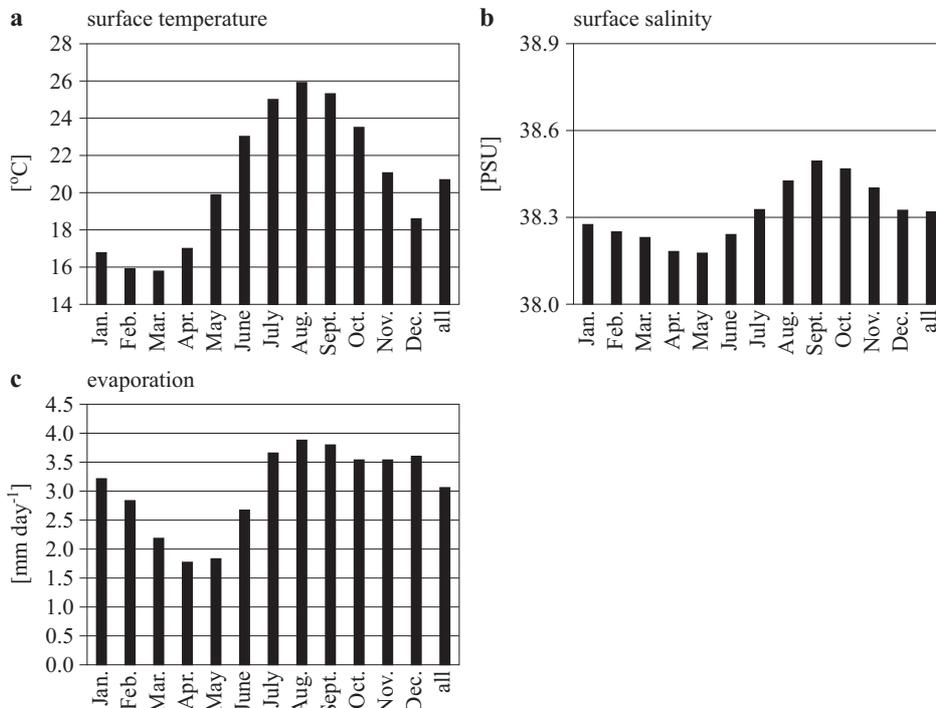
Figure 9. Monthly average a) surface temperatures, b) salinities and c) evaporation rates

Another test of the model simulations was to investigate the water mass structure throughout the EMB. By comparing modelled and observed ocean data, an independent test of the approach could be performed. The results are presented in Figure 10a, in which three water masses, i.e. Atlantic water (AW) at the surface, Levantine intermediate water (LIW) at an intermediate

a

b
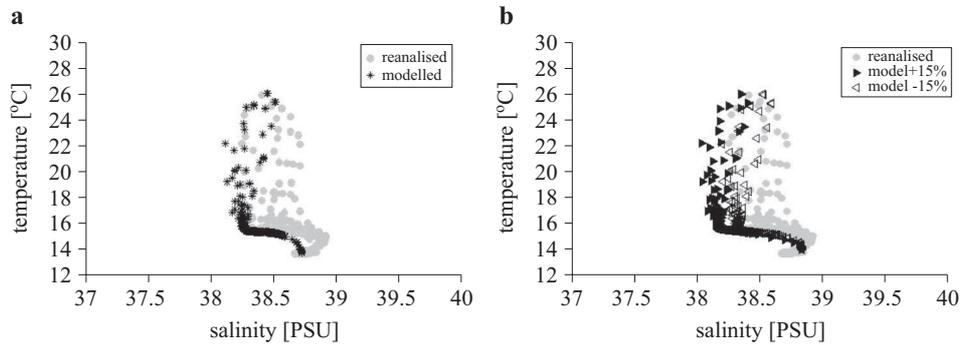
Figure 10. Monthly calculated and reanalysed temperatures and salinities of the Eastern Mediterranean Basin

a sea surface temperature

b sea surface salinity
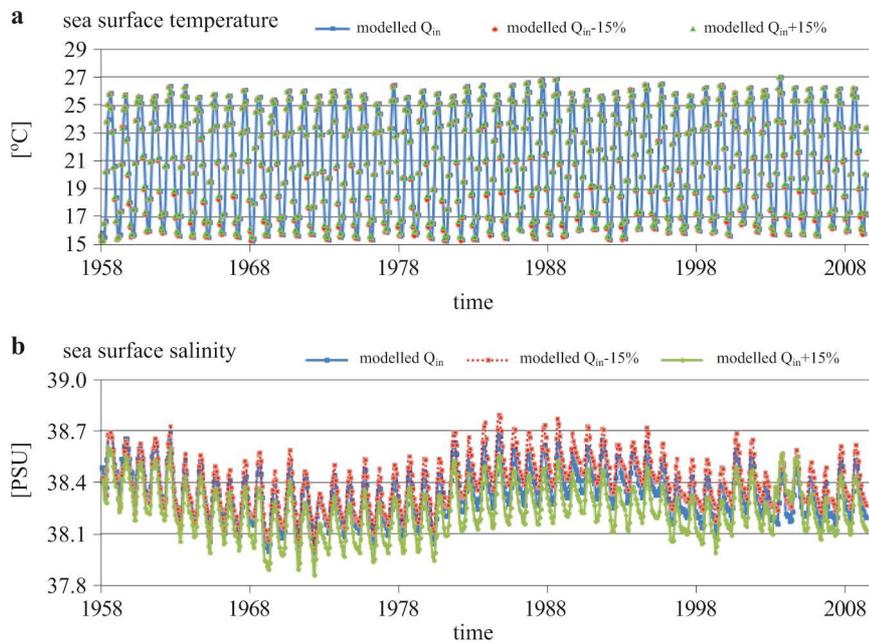
Figure 11. Illustrations of modelled Eastern Mediterranean Basin a) surface temperatures and b) surface salinities with changes in the Sicily Channel volume flows

depth, and deep water, can be identified in the T–S diagram. Deep water masses are more obvious in the observations than in the modelled data owing to the coarse model resolution.

To analyse the sensitivity of the PROBE-EMB model to changes in inflows, two sensitivity runs were performed by adding $\pm 15\%$ of the mean value of Q_{in} (1.16×10^6 m^3 s^{-1}) to all Q_{in} values (Figures 10 and 11).

We conclude that changes in Q_{in} within the $\pm15\%$ range bring about only minor changes in the vertical distribution of salinity and temperature, which indicates that the assumption of extrapolating the 4-year period of the AVISO database over the whole period studied is acceptable.

3.3. Modelled water components for the Eastern Mediterranean Basin

The water balance of EBM is controlled by the Sicily Channel exchange (Q_{in} and Q_{out}), river runoff (Q_f), and net precipitation, i.e. the difference between the precipitation and evaporation rates (equation (1)). The various water balance components, except precipitation and river runoff, are modelled using the PROBE-EMB model. Table 1 and Figure 12 show the estimated monthly and annual mean water balances of the EMB averaged over 52 years. Moreover, the annual mean of the difference between inflow and outflow and the net precipitation flow, i.e. $A_s(P-E)$, are illustrated together with Q_f in Figure 13.

Table 1. Modelled monthly and annual mean water balance of the Eastern Mediterranean Basin averaged over 52 years

Months	Q_f	P	E	$A_s(P-E)$	Q_{in}	Q_{out}
	$[10^6 \text{ m}^3 \text{ s}^{-1}]$	[mm day^{-1}]		$[10^6 \text{ m}^3 \text{ s}^{-1}]$		
January	0.012	2.80	3.24	−0.009	1.03	1.02
February	0.013	2.27	2.87	−0.011	1.18	1.20
March	0.015	1.60	2.23	−0.012	1.20	1.19
April	0.018	0.95	1.79	−0.016	1.43	1.42
May	0.016	0.59	1.85	−0.024	1.09	1.06
June	0.010	0.41	2.70	−0.044	1.19	1.15
July	0.007	0.30	3.70	−0.066	1.09	1.04
August	0.006	0.39	3.91	−0.068	1.03	0.95
September	0.007	1.06	3.84	−0.054	1.04	0.99
October	0.008	1.89	3.58	−0.033	1.20	1.17
November	0.010	2.60	3.57	−0.019	1.22	1.20
December	0.012	3.27	3.63	−0.007	1.28	1.31
annual	0.011	1.50	3.08	−0.030	1.16	1.14

The results indicate that the in- and outflows are of the order of $10^6 \text{ m}^3 \text{ s}^{-1}$, while the difference between them is approximately two orders less. This difference between the in- and outflows was balanced mainly by net precipitation and river runoff, the net precipitation being approximately 3 times greater than the river discharge. The water balance was thus mainly controlled by the in- and outflows through the Sicily Channel and by the net precipitation. The results also indicate that the

a

b

c
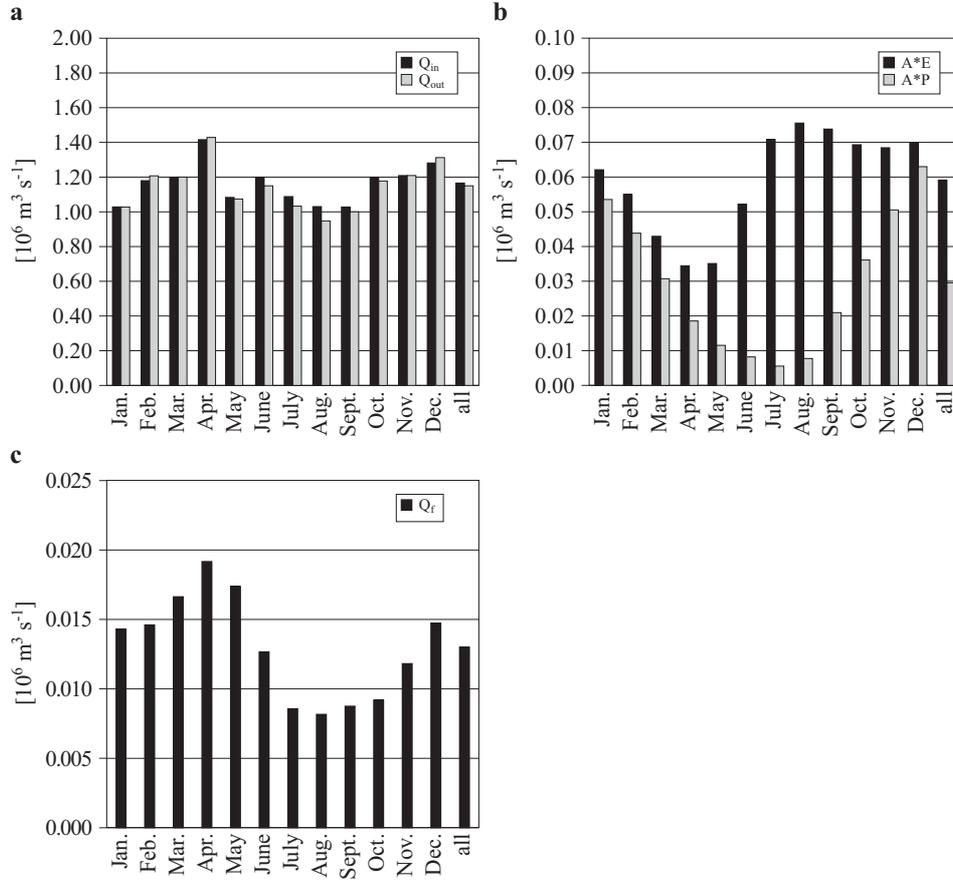
Figure 12. Monthly calculated a) in- and outflows, b) precipitation and evaporation rates and c) river runoff for the Eastern Mediterranean Basin

maximum monthly mean value of Q_{in} occurred in April and was 1.43×10^6 m^3 s^{-1}, while the maximum monthly mean value of Q_{out} also occurred in April and was 1.42×10^6 m^3 s^{-1}. The monthly net precipitation reached a maximum in August at 0.068×10^6 m^3 s^{-1} and a minimum in December at 0.007×10^6 m^3 s^{-1}. Depending on monthly values, the difference between the in- and outflows indicates a positive trend of 3.33×10 m^3 s^{-1} yr^{-1}, while net precipitation displays a negative trend of -2.2×10 m^3 s^{-1} yr^{-1}. The negative trend in net precipitation was due to a negative evaporation trend of approximately -1.6×10 m^3 s^{-1} yr^{-1} together with a negative precipitation trend of -3.8×10 m^3 s^{-1} yr^{-1}. The freshwater discharge into the EMB (i.e. via rivers of the Eastern Basin plus the Black Sea) also displayed a negative trend of -2.4×10 m^3 s^{-1} yr^{-1}, explained mainly by the building of the Aswan High Dam in 1964 (which reduced the River
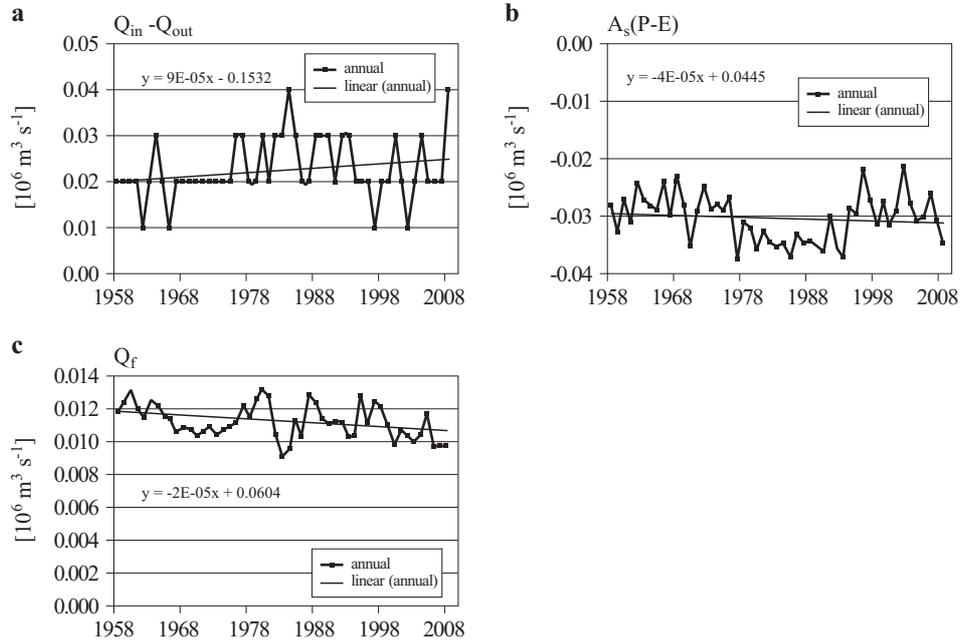
Figure 13. Annual calculated mean of the water balance components for the Eastern Mediterranean Basin: a) difference between in- and outflows, b) net evaporation rates and c) river discharge

Nile's discharge by approximately half) and decreasing net precipitation over the Black Sea Basin (the decrease in Black Sea discharge was estimated to be approximately -9.8×10 m^3 s^{-1} yr^{-1}). The negative trends in the freshwater components indicating increasing EMB salinity agree with the findings of Skliris et al. (2007). The EMB monthly mean river runoff ranged from 0.006×10^6 m^3 s^{-1} in August to 0.018×10^6 m^3 s^{-1} in April, with an annual average of 0.011×10^6 m^3 s^{-1}. Over the studied 52-year period, $Q_{in} - Q_{out}$ averaged $0.023 \pm 0.84 \times 10^6$ m^3 s^{-1}, while $A_s(P - E)$ averaged $-0.03 \pm 0.04 \times 10^6$ m^3 s^{-1}, the difference being balanced by the river discharge (Table 1).

3.4. Modelled heat balance components

The monthly means of the heat budget components are presented in Table 2 and Figure 14, while the annual means of F_n, F_s^o and F_{loss} are presented in Figure 15. The heat balance simulations indicate that the heat loss from the open sea was almost balanced by the solar radiation to the open water surface. Heat loss from the open sea ranged from 134.9 W m^{-2} to 229.8 W m^{-2}, while solar radiation to the open water surface ranged from -300.3 W m^{-2} in July to -73.3 W m^{-2} in December. The total heat flux

Table 2. Estimated monthly and annual means of heat balance components

| Months	F_h	F_e	F_l	F_s^o	F_{loss}
			$[\text{W m}^{-2}]$		
January	41.10	93.69	82.55	−83.03	134.33
February	34.76	82.91	79.49	−116.21	80.95
March	22.84	64.34	72.91	−168.11	−8.01
April	14.07	51.72	69.08	−224.78	−89.91
May	12.48	53.37	71.01	−269.57	−132.71
June	17.17	78.02	78.65	−297.70	−123.86
July	22.18	106.93	83.03	−300.32	−88.18
August	24.41	113.26	86.09	−268.42	−44.65
September	26.49	111.06	88.89	−208.78	17.66
October	28.11	103.56	84.44	−138.39	77.71
November	33.83	103.25	80.92	−90.43	127.57
December	41.76	104.89	83.15	−73.71	156.08
annual	26.58	88.99	80.01	−186.88	8.70
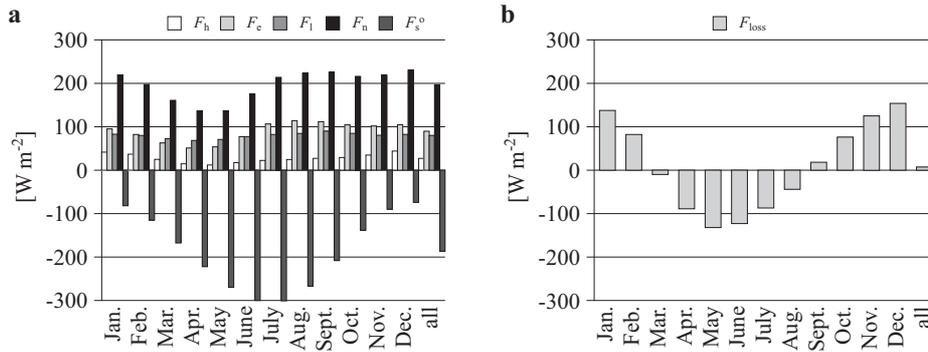
Figure 14. Monthly calculated heat fluxes for the Eastern Mediterranean basin: net heat loss from the sea (F_n), sensible heat flux (F_h), latent heat flux (F_e), net long-wave radiation (F_l), a) solar radiation to the open water surface (F_s^o; negative fluxes indicate fluxes into the water body) and b) heat loss through the open water surface (F_{loss})

from the EMB surface was negative (indicating fluxes into the water body) from March to August, while it was positive in the rest of the year. Latent heat flux and net long-wave radiation are more important than sensible heat flux in controlling the variability of heat loss from the open sea. The annual average value of F_{loss} was 8.7 W m^{-2}, which needs to be balanced by the difference in heat transported by the in- and outflowing water. During the study period, the annual average values of F_n and F_s^o were 195.6 W m^{-2} and −186.9 W m^{-2} respectively. Modelled F_n data indicate an increasing trend of 0.07 W m^{-2} yr^{-1}, while F_s^o data indicate
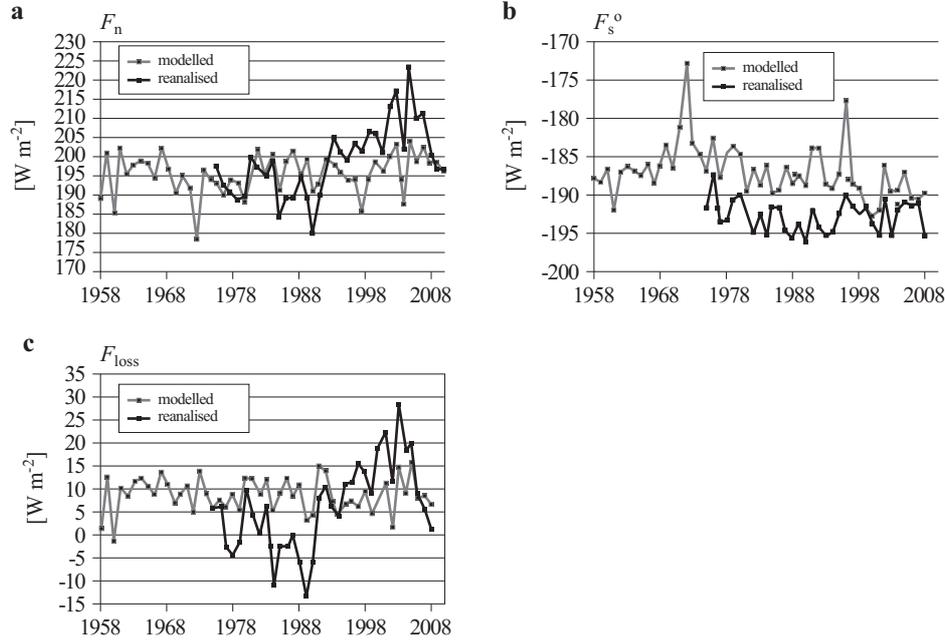
Figure 15. Annual means of the calculated and reanalysed heat balance components for the Eastern Mediterranean Basin: a) net heat loss from the sea (F_n), b) solar radiation to the open water surface (F_n) and c) total heat loss through the open water surface (F_{loss}). The modelled values are taken from the present model study, while the reanalysed data were extracted from the ECMWF meteorological database

a decreasing trend of approximately 0.07 W m^{-2} yr^{-1}. This indicates an increase in solar radiation into the water body and an increase in net heat loss, probably due to reduced total cloud cover rates. Moreover, the figures indicate a close relationship between the ECMWF meteorological data and the present modelled heat balance components, i.e. F_n, F_s^o and F_{loss}, with biases of 4, 2.7 and 3.2 W m^{-2} respectively.

In addition, the positive value of the annual average F_{loss}, 8.7 W m^{-2}, implies that the EMB imports heat from the Western Basin (Table 2). Using equation (2), assuming a steady state, and averaging over the studied period, the heat conservation can be written as

$$F_{\text{loss}}A_s \approx \rho_o c_p Q_{in} T_{in} - \rho_o c_p Q_{out} T_{out}$$

with A_s equal to 1.67×10^{12} m^2, c_p equal to 4200 J(kg °C)$^{-1}$, and calculating the long-term mean in- and outflows and associated temperatures from the model (Q_{in}, T_{in}, Q_{out}, $T_{out} = 1.16 \times 10^6$ m^3 s^{-1}, 18.1°C, 1.14×10^6 m^3 s^{-1}, 15.32°C), we obtain an average F_{loss} of 9 W m^{-2}; this is in accordance with

the value presented in Table 2 and indicates that the net heat loss at the surface was compensated for by the heat transported through the Sicily Channel.

Finally, to evaluate the modelling approach, the heat and salt contents of the whole EMB water column changes were simulated using the PROBE-EMB model and compared with observations from the MEDAR ocean database (Figure 16). The comparison indicates a close correlation, with the calculated total heat content deviating approximately 1% from the MEDAR value. For the salt content, the modelled value deviates by less than 0.3% from the MEDAR value. The PROBE-EMB can realistically reproduce the water and heat balances of the EMB.
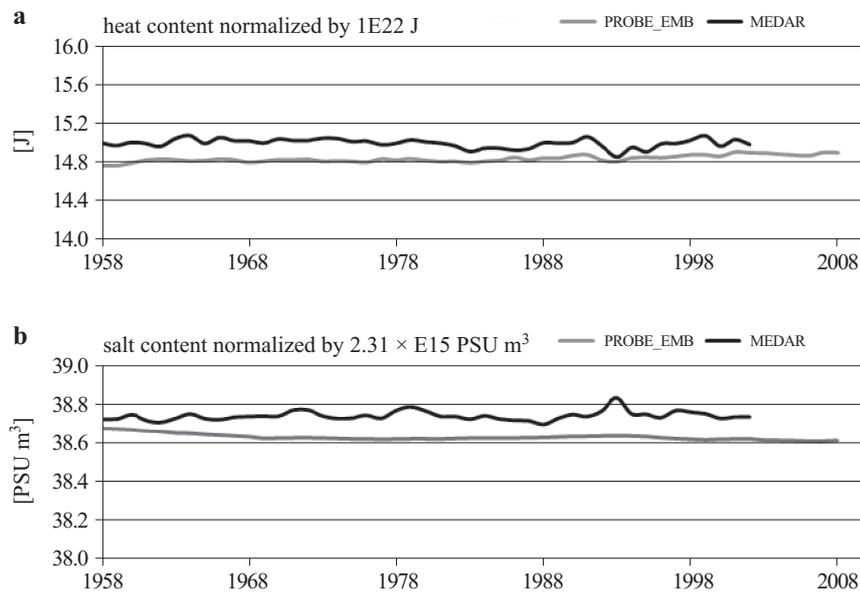
Figure 16. Yearly calculated heat and salt contents based on the model and on observations of the Eastern Mediterranean Basin

4. Discussion

The connection between atmospheric conditions over the Mediterranean Basin and the large-scale atmospheric circulation in the Northern Hemisphere is generally strong, for example, as represented by the North Atlantic Oscillation (NAO). There is a significant link ($R = 0.45$, $n = 52$) between winter precipitation over the EMB and the NAO (data not shown but available from the National Oceanic and Atmospheric Administration – NOAA – database). Moreover, there is a link ($R = 0.3$, $n = 52$) between

winter NAO and winter evaporation. Wet (dry) winters are associated with positive (negative) NAO index values. On the other hand, negative (positive) NAO index values are associated with increased (decreased) evaporation rates in the winter. Changes in the NAO index greatly affect the winter water and heat balances of the EMB, which is in agreement with, for example, the results of Turkes (1996a,b).

The study analyses the large-scale features of the EMB using ocean modelling and available meteorological and hydrological datasets. Local features (e.g., the Eastern Mediterranean Transient, EMT) are therefore not included. It is a budget-type method building on horizontal averaging, i.e. strong local forcing might trigger convections that reach the bottom, while the same forcing averaged over the whole basin may have a minor influence. In the future, we will model the EMB as a number of sub-basins and also address local EMB features that may influence the water and heat balances. For example, the Southern Aegean Basin is significantly affected by deep water formation and needs to be considered when modelling deep water formation.

The individual terms of the water and heat balances were analysed together with how the climate change signals affect the heat and water cycles. Individual water and heat component values are presented in figures and tables. There were strong monthly and interannual variations in most of the water and heat balance components. The results indicate that atmospheric climate conditions, rather than exchange through the Sicily Channel, dominated the heat and water balances of the Eastern Mediterranean.

Using satellite dynamic height observations across the Sicily Channel, together with the assumptions of geostrophic flows and volume conservation, the exchanges through the channel were realistically modelled. The calculated water inflow ($Q_{in} = 1.05 \pm 0.35 \times 10^6$ m^3 s^{-1}) to the EMB was in good agreement with the results of Béranger et al. (2002) and Buongiorno Nardelli et al. (2006), but greater than those of Ferjani & Gana (2010) by approximately 0.6×10^6 m^3 s^{-1}, partly due to the better resolution of the Sicily channel in the present study.

An important trend in the water balance components was the reduced freshwater discharge into the EMB, which implies increasing salinity. This was partly due to the decrease in the River Nile's discharge into the EMB after the building of Aswan High Dam and partly due to a decrease in the Black Sea discharge as a result of a negative net precipitation trend over that sea. The decreased Black Sea discharge into the EMB will be of major interest in future studies, as it will influence the Aegean Sea water dynamics, especially the Eastern Mediterranean Transient phenomena.

Modelled long-term surface temperature and salinity followed the re-analysed data, with respective biases of $-0.4°$C and -0.004 PSU. Modelled sea surface temperature showed a positive trend of $0.012°$C yr^{-1} over the period 1958–2008. This warming trend became stronger ($0.03°$C yr^{-1}) for the years 1985–2008. On the other hand, satellite data set (Skliris et al. 2012) show a $0.04°$C yr^{-1} rise in EMB sea surface temperature, which agrees with our result. Yearly temperature and salinity cycles for the different three layers (surface, intermediate and deep) were also well simulated. Reanalysed and modelled water mass structure and heat balance components displayed good agreement, indicating that the air-sea interaction and turbulent mixing were realistically simulated. Only horizontally averaged layer quantities for the whole Eastern Mediterranean Basin were considered, and deep water convection was simply modelled using the mixing process.

In Table 3 a comparison is given between different estimates of the net precipitation rates over EMB. The present modelled net precipitation rates over the years 1958–2008 showed a negative trend of -0.007 mm day^{-1} yr^{-1} and with yearly averaged values of -1.5 ± 1.2 mm day^{-1}, while reanalysed net precipitation shows no changes with yearly average values of -1.75 ± 0.8 mm day^{-1} yr^{-1}. During the period 1985–2008, our modelled net precipitation rates showed a small positive trend of 0.01 mm day^{-1} yr^{-1}, but the reanalysed data did not display any trend. The yearly average values of modelled and reanalysed net precipitation over the years 1985–2008 were -1.55 ± 1.2 and -1.75 ± 0.8 mm day^{-1} respectively. Romanou et al. (2010) used satellite-derived ocean surface flux products (HOAPS-3) in estimating the variability of E and P over EMB during 1988–2005. They found a negative net precipitation trend of 0.04 mm day^{-1} yr^{-1} with a yearly average of -3.5 mm day^{-1}. Mariotti et al. (2002) reported mean yearly values of Mediterranean net precipitation rates ranging from -1.3 to -1.9 mm day^{-1} over the years 1979–1993. The different estimates do not differ too much, even though quite different methods have been used and our calculations support the reanalysed data set.

Table 3. Net precipitation rates based on different estimates

Source	Net precipitation (1958–2008)		Net precipitation (1985–2008)	
	Mean [mm day^{-1}]	Trend [mm day^{-1} yr^{-1}]	Mean [mm day^{-1}]	Trend [mm day^{-1} yr^{-1}]
present study	-1.5 ± 1.2	-0.007	-1.55 ± 1.2	0.01
Romanou et al. (2010)	$-$	$-$	-3.5	-0.04
reanalysed	-1.75 ± 0.8	none	-1.75 ± 0.8	none

The water balance in the Eastern Mediterranean basin was found to be controlled by (in order of importance): (1) the net precipitation rates (annual average of -0.03×10^6 m^3 s^{-1}), (2) the difference between the in- and outflows through the Sicily Channel (annual average of 0.02×10^6 m^3 s^{-1}), and (3) the river runoff (annual average of 0.01×10^6 m^3 s^{-1}). The heat balance was controlled by (in order of importance): (1) the heat loss from the water surface (annual average of 195 W m^{-2}), (2) the solar radiation into the sea (annual average of -187 W m^{-2}), and (3) the heat flow through the Sicily Channel, the first two displaying evidence of both climate trends. An annual net heat loss of approximately 8.7 W m^{-2} was balanced by the net heat flow through the Channel. The study demonstrated that ocean modelling, together with available meteorological and river runoff data, provides a powerful method for analysing heat and water cycles. The water and heat balances, together with trend analysis of a long time series, will be used as climate change tools in future studies.

Acknowledgements

References

Béranger K., Mortier L., Crépon M., 2002, *Seasonal transport variability through Gibraltar, Sicily and Corsica Straits*, The 2nd Meeting on the Physical Oceanography of Sea Straits, 15–19 April 2002 (pp. 77–81), Villefranche, France.

Bodin S., 1979, *A predictive numerical model of the atmospheric boundary layer based on the turbulent energy equation*, Norrkoping, Sweden: SMHI (Report: Meteorology and Climatology No. 13, SE-601 76).

Buongiorno Nardelli B., Cavalieri O., Rio, M.H., Santoleri R., 2006, *Subsurface geostrophic velocities inference from altimeter data: Application to the Sicily Channel (Mediterranean Sea)*, J. Geophys. Res., 111, C04007, doi:10.1029/2005JC003191.

Burchard H., Petersen O., 1999, *Models of turbulence in the marine environment: a comparative study of two-equation turbulence models*, J. Marine Syst., 21 (1–4), 29–53.

Ferjani D., Gana S., 2010, *Seasonal circulation and mass flux estimates in the western Sicily Strait derived from a variational inverse section model*, Deep Sea Res. Pt. I, 57, 1177–1191.

Hasselmann S., Hasselmann K., Bauer E., Janssen P. A. E. M., Komen G. J., Bertotti L., Lionelli P., Guillome A., Cardone V. C., Greenwood J. A., Reistad M., Zambresky L., Ewing J. A., 1988, *The WAM Model – a third generation ocean wave prediction model*, J. Phys. Oceanogr., 18 (12), 1775–1810.

Jerlov N. G., 1968, *Optical oceanography*, Oceanography Ser., Vol. 5, Elsevier, Amsterdam.

Launiainen J., 1995, *Derivation of the relationship between the Obukhov stability parameter and the bulk Richardson number for flux profiles*, Bound.-Lay. Meteorol., 76 (1–2), 165–179, doi:10.1007/BF00710895.

Ludwig W., Dumont E., Meybeck M., Heussner S., 2009, *River discharges of water and nutrients to the Mediterranean and Black Sea: Major drivers for ecosystem changes during past and future decades?*, Prog. Oceanogr., 80 (3–4), 199–217, doi:10.1016/j.pocean.2009.02.001.

Malanotte-Rizzoli P., Manca B., d'Alcala M., Theocharis A., Brenner S., Budillon G., Ozsoy E., 1999, *The eastern Mediterranean in the 80s and in the 90s: The big transition in the intermediate and deep circulations*, Dynam. Atmos. Oceans, 29 (2–4), 365–395, [http:/dx.doi.org/10.1016/S0377-0265(99)00011-1].

Mariotti A., Struglia M., Zeng N., Lau K., 2002, *The hydrological cycle in the Mediterranean region and implications for the water budget of the Mediterranean Sea*, J. Climate, 15, 1674–1690, [http://dx.doi.org/10.1175/1520-0442(2002)015<1674:THCITM>2.0.CO;2].

Nixon S. W., 2003, *Replacing the Nile: are anthropogenic nutrients providing the fertility once brought to the Mediterranean by a great river?*, Ambio, 32 (1), 30–39.

Omstedt A., 2011, *Guide to process based modelling of lakes and coastal seas*, Springer-Praxis books in Geophysical Sciences, Springer-Verlag, Berlin, Heidelberg, doi:10.1007/978-3-642-17728-6.

Omstedt A., Axell L. B., 2003, *Modeling the variations of salinity and temperature in the large gulfs of the Baltic Sea*, Cont. Shelf. Res., 23 (3–4), 265–294, doi:10.1016/S0278-4343(02)00207-8.

Omstedt A., Nohr C., 2004, *Calculating the water and heat balances of the Baltic Sea using ocean modelling and available meteorological, hydrological and ocean data*, Tellus, 56A, 400–414, doi:10.1111/j.1600-0870.2004.00070.x.

Rixen J., Beckers M., Levitus S., Antonov J., Boyer T., Maillard C., Fichaut M., Balopoulos E., Iona S., Dooley H., Garca M. J., Manca B., Giorgetti A., Manzella G., Mikhailov N., Pinardi N., Zavatarelli M., 2005, *The Western Mediterranean deep water: A proxy for climate change*, Geophys. Res. Lett., 32, L12608, doi:10.1029/2005GL022702.

Roether W., Schlitzer R., 1991, *Eastern Mediterranean deep water renewal on the basis of chlorofluoromethane and tritium data*, Dynam. Atmos. Oceans, 15, 333–354, [http://dx.doi.org/10.1016/0377-0265(91)90025-B].

Romanou A., Tselioudis G., Zerefos C., Clayson C., Curry J., Andersson A., 2010, *Evaporation-precipitation variability over the Mediterranean and the Black Seas from satellite and reanalysis estimates*, J. Climate, 23 (19), 5268–5287, [http://dx.doi.org/10.1175/2010JCLI3525.1].

Skliris N., Sofianos S., Gkanasos A., Mantziafou A., Vervatis V., Axaopoulos P., Lascaratos A., 2012, *Decadal scale variability of sea surface temperature in the Mediterranean Sea in relation to atmospheric variability*, Ocean Dynam., 62 (1), 13–30, doi:10.1007/s10236-011-0493-5.

Skliris N., Sofianos S., Lascaratos A., 2007, *Hydrological changes in the Mediterranean Sea in relation to changes in the freshwater budget: A numerical modelling study*, J. Marine Syst., 65 (1–4), 400–416.

Sorgente R., Drago A. F., Ribotti A., 2003, *Seasonal variability in the Central Mediterranean Sea circulation*, Ann. Geophys., 21, 299–322.

Stanev E. V., Le Traon P. Y., Peneva E. L., 2000, *Sea level variations and their dependency on meteorological and hydrological forcing: Analysis of altimeter and surface data for the Black Sea*, J. Geoph. Res., 105, C7, 17203–17216.

Stanev E., Peneva E. L., 2002, *Regional sea level response to global climatic change: Black Sea examples*, Global Planet. Change, 32 (1), 33–47, [http://dx.doi.org/10.1016/S0921-8181(01)00148-5].

Stansfield K., Smeed D. A., Gasparini G. P., 2002, *The path of the overflows from the sills in the Sicily Strait*, The 2nd Meeting on the Physical Oceanography of Sea Straits, 15–19 April 2002 (pp. 211–215), Villefranche, France.

Turkes M., 1996a, *Meteorological drought in Turkey: A historical perspective, 1930–1993*, Drought Network News, 8, 17–21, [http://digitalcommons.unl.edu/droughtnetnews/84].

Turkes M., 1996b, *Spatial and temporal analysis of annual rainfall variations in Turkey*, Int. J. Climatol., 16, 1057–1076.

Zervakis V., Georgopoulos D., Drakopoulos P., 2000, *The role of the North Aegean in triggering the recent Eastern Mediterranean climatic changes*, J. Geophys. Res., 105, C11, 26103–26116, doi:10.1029/2000JC900131.

Appendix A1. Model description

The Eastern Mediterranean Basin (EMB) is influenced by various physical processes (see the Introduction). A useful initial approach is to model the EMB as one basin and separately examine the effects of local factors and of interactions with surrounding basins (i.e. the Tyrrhenian and Black Sea basins). The modelling starts by using the PROBE equation solver, a well-documented and freely available program for studies of lakes and coastal seas (Omstedt 2001). This equation solver is based on the finite volume method and can easily solve a large number of equations for networks of sub-basins. In the present version, PROBE-EMB version 1.0, the EMB is treated as one basin coupled to surrounding basins by in- and outflows; the program is freely available from the present authors.

Mathematical formulation

The transport equations for momentum read:

$$\frac{\partial \rho U}{\partial t} + W \frac{\partial \rho U}{\partial z} = \frac{\partial}{\partial z} \left[\frac{\mu_{eff}}{\rho} \frac{\partial \rho U}{\partial z} \right] + f \rho V, \tag{1}$$

$$\frac{\partial \rho V}{\partial t} + W \frac{\partial \rho V}{\partial z} = \frac{\partial}{\partial z} \left[\frac{\mu_{eff}}{\rho} \frac{\partial \rho V}{\partial z} \right] - f \rho U, \tag{2}$$

$$W = \frac{(Q_{in} - Q_{out})}{\text{Area}}, \tag{3}$$

where U and V are the current components in the easterly and northerly directions respectively, W the vertical velocity calculated from the differences between in- and outflows (U, V and W are horizontally averaged velocities), f the Coriolis parameter, ρ the sea water density, μ_{eff} the effective dynamic viscosity, Q_{in}, Q_{out} and A the inflows, outflows and areas at different levels respectively, z the vertical coordinate (positive upward) and t time.

Equations (1)–(3) apply a transient Ekman flow model with vertical velocity due to in- and outflows and including density effects. As the in- and outflows may act at different levels, they generate vertical motions in the model.

The water-air boundary conditions are:

$$\tau_{ax} = \frac{\mu_{eff}}{\rho} \frac{\partial \rho U}{\partial z}, \tag{4a}$$

$$\tau_{ay} = \frac{\mu_{eff}}{\rho} \frac{\partial \rho V}{\partial z}, \tag{4b}$$

where τ_{ax} and τ_{ay} denote the eastward and northward wind stress components respectively, calculated using a standard bulk formulation:

$$\tau_{ax} = \rho_a C_D U_a W_a, \tag{5a}$$

$$\tau_{ay} = \rho_a C_D V_a W_a, \tag{5b}$$

where ρ_a (1.3 kg m^{-3}) is the air density, C_D the air drag coefficient, U_a and V_a the wind components in the x and y directions respectively, and W_a the wind speed $= \sqrt{U_a^2 + V_a^2}$. The air drag coefficient for the natural atmosphere (C_{DN}) is calculated according to Hasselmann et al. (1988) by

$$C_{DN} = [0.8 + 0.065 \max(W_a,\, 7.5)] \times 10^{-3}. \tag{5c}$$

The roughness lengths for momentum (Z_o), heat (Z_H) and humidity (Z_E) are assumed to be dependent on the neutral values as

$$Z_o = \frac{z_{ref}}{\exp\left(\dfrac{\kappa}{\sqrt{C_{DN}}}\right)}, \tag{5d}$$

$$Z_H = \frac{z_{ref}}{\exp\left(\dfrac{\kappa\sqrt{C_{DN}}}{C_{HN}}\right)}, \tag{5e}$$

$$Z_o = \frac{z_{ref}}{\exp\left(\dfrac{\kappa\sqrt{C_{DN}}}{C_{EN}}\right)}, \tag{5f}$$

where Z_{ref} is the reference height ($= 10$ m), $\kappa(= 0.4)$ is von Karman's constant, $C_{HN}(= 1.14 \times 10^{-3})$ is the neutral bulk coefficient for the sensible heat flux and $C_{EN}(= 1.12 \times 10^{-3})$ is the neutral bulk coefficient for the latent heat flux. According to Launiainen (1995), the stability dependence of the bulk coefficients is:

$$C_D = \frac{\kappa^2}{\left[\ln\left(\dfrac{Z_{ref}}{Z_o}\right) - \psi_m\right]^2}, \tag{5g}$$

$$C_H = \frac{\kappa^2}{\left[\ln\left(\dfrac{Z_{ref}}{Z_o}\right) - \psi_m\right]\left[\ln\left(\dfrac{Z_{ref}}{Z_H}\right) - \psi_h\right]}, \tag{5h}$$

$$C_H = \frac{\kappa^2}{\left[\ln\left(\dfrac{Z_{ref}}{Z_o}\right) - \psi_m\right]\left[\ln\left(\dfrac{Z_{ref}}{Z_E}\right) - \psi_h\right]}, \tag{5i}$$

where ψ_m, (ψ_h) are the integrated forms of the non-dimensional gradients of momentum (heat). They are calculated as follows:

For stable and neutral conditions the Richardson number (R_b) is used to define a stable ($R_b > 0$) and an unstable condition ($R_b < 0$):

$$R_b = \frac{gZ_{ref}(T_a - T_s)}{(T_s + 273.15)W_a^2}. \tag{5j}$$

The non-dimensional fraction (ς) is calculated by knowing the air temperature at 2 m height (T_a) and the sea surface temperature (T_s):

$$\varsigma = \left[R_b\left(1.18\ln\left(\frac{Z_{ref}}{Z_o}\right) - 1.5\ln\left(\frac{Z_o}{Z_H}\right) - 1.37\right)\right] +$$
$$+ \left[R_b^2\left(1.891\ln\left(\frac{Z_{ref}}{Z_o}\right) + 4.22\right)\right], \tag{5k}$$

where L is the Monin-Obukov length. During a strongly stable situation, ς is less than or equal to 0.5, and

$$\psi_m \approx \psi_h = -\left(\frac{c\psi_2 c\psi_3}{c\psi_4}\right) - (\varsigma c\psi_1) - \left(\left(c\psi_2\left(\varsigma - \frac{c\psi_3}{c\psi_4}\right)\right)\exp(-\varsigma c\psi_4)\right), \tag{5l}$$

where $c\psi_1$, $c\psi_2$, $c\psi_3$ and $c\psi_4$ are 0.7, 0.75, 5 and 0.35 respectively.

For unstable conditions ς is calculated as

$$\varsigma = R_b\left[\frac{\ln^2(Z_{ref}/Z_o)}{\ln(Z_{ref}/Z_H)} - 0.55\right]. \tag{5m}$$

For strongly unstable conditions, ς is larger than -5; the integrated forms of the gradients are then given by

$$\psi_m = 2\ln\left(\frac{1 + (1 - 16\varsigma)^{0.25}}{2}\right) +$$
$$+ \ln\left(\frac{1 + (1 - 16\varsigma)^{0.5}}{2}\right) - 2\arctan((1 - 16\varsigma)^{0.25}) + \frac{\pi}{4}, \tag{5n}$$

$$\psi_h = 2\ln\left(\frac{1 + (1 - 16\varsigma)^{0.5}}{2}\right). \tag{5o}$$

The conservation equation for heat reads:

$$\frac{\partial \rho c_p T}{\partial t} + W\frac{\partial \rho c_p T}{\partial z} = \frac{\partial}{\partial z}\left[\frac{\mu_{eff}}{\rho\sigma_{effT}}\frac{\partial(\rho c_p T)}{\partial z}\right] + \Gamma_{sum} + \Gamma_h, \tag{6}$$

where T and c_p are the temperature of sea water and the heat capacity (4200 J Kg^{-1} K^{-1}), respectively, σ_{effT} the turbulent Prandtl number (set

equal to one in the present version of the model), and Γ_{sum} and Γ_h the respective source terms associated with solar radiation in- and outflows.

The source terms Γ_{sum} and Γ_h are given by

$$\Gamma_{\text{sum}} = F_s^w (1 - \eta_1) e^{-\beta(D-z)}, \tag{7a}$$

$$\Gamma_h = \rho c_p \left(\frac{Q_{in} T_{in}}{\Delta V_{in}} - \frac{Q_{out} T_{out}}{\Delta V_{out}} \right), \tag{7b}$$

where F_s^w is the short-wave radiation through the water surface, $\eta_1 (= 0.4)$ the infrared fraction of short-wave radiation trapped in the surface layer, β the bulk absorption coefficient of the water (0.3 m^{-1}), D the total depth, T_{in} and T_{out} the respective temperatures of the in- and outflowing water, and ΔV_{in} and ΔV_{out} the respective volumes of the grid cells at the in- and outflow levels.

The boundary condition at the surface for heat reads:

$$F_{\text{net}} = \frac{\mu_{eff}}{\rho \sigma_{effT}} \frac{\partial(\rho C_p T)}{\partial z}, \tag{8a}$$

$$F_{\text{net}} = F_h + F_e + F_l + \delta F_s^W, \tag{8b}$$

where F_h is the sensible heat flux, F_e the latent heat flux, F_l the net long-wave radiation and δF_s^W the short-wave radiation part absorbed in the surface layer.

The conservation equation for salinity reads:

$$\frac{\partial S}{\partial t} + W \frac{\partial S}{\partial z} = \frac{\partial}{\partial z} \left[\frac{\mu_{eff}}{\rho \sigma_{effS}} \frac{\partial S}{\partial z} \right] + \Gamma_S, \tag{9a}$$

$$\Gamma_S = \frac{Q_{in} S_{in}}{\Delta V_{in}} - \frac{Q_{out} S_{out}}{\Delta V_{out}} - \frac{Q_f S_{sur}}{\Delta V_{sur}}, \tag{9b}$$

where Γ_S is the source term associated with in- and outflows, σ_{effS} the turbulent Schmidt number (equal to one), Q_f the river discharge to the basin, S_{in} and S_{out} the salinity of the in- and outflowing water respectively, S_{surf} the sea surface salinity, and ΔV_{sur} the volume of the upper surface grid cell.

The boundary conditions at the surface for salinity (S) read:

$$\frac{\mu_{eff}}{\rho \sigma_{effS}} \frac{\partial S}{\partial z} = F_{\text{salt}}, \tag{10a}$$

$$F_{\text{salt}} = S_s (P - E), \tag{10b}$$

where F_{salt} is the salt flux associated with net precipitation, S_s the surface salinity and P the precipitation rate (calculated from given values). Evaporation (E) is calculated by the model as

$$E = \frac{F_e}{L_e \rho_o}, \tag{10c}$$

where F_e is the latent heat flux, L_e the latent heat of evaporation, and ρ_o the reference density of sea water (i.e. 10^3 kg m^{-3}). It should be noted that equation (10a) connects the water and heat balances.

The turbulence model

The vertical turbulent transports in the surface boundary layer are calculated using the well-known k-ε model (e.g. Burchard & Petersen 1999), a two-equation model of turbulence in which transport equations for the turbulent kinetic energy k and its dissipation rate ε are calculated. The transport equations for k and ε read:

$$\frac{\partial k}{\partial t} + W \frac{\partial k}{\partial z} = \frac{\partial}{\partial z}\left[\frac{\mu_{eff}}{\rho \sigma_k}\frac{\partial k}{\partial z}\right] + P_s + P_b - \varepsilon, \tag{11}$$

$$\frac{\partial \varepsilon}{\partial t} + W \frac{\partial \varepsilon}{\partial z} = \frac{\partial}{\partial z}\left[\frac{\mu_{eff}}{\rho \sigma_\varepsilon}\frac{\partial \varepsilon}{\partial z}\right] + \frac{\varepsilon}{k}[c_{\varepsilon 1}P_s + c_{\varepsilon 3}P_b - c_{\varepsilon 2}\varepsilon], \tag{12}$$

where P_s and P_b are the production/destruction due to shear and stratification respectively, σ_k (=1) the Schmidt number for k, and σ_ε (=1.11) the Schmidt number for ε. The various terms are modelled as

$$P_s = \frac{\mu_{eff}}{\rho}\left[\left(\frac{\partial U}{\partial z}\right)^2 + \left(\frac{\partial V}{\partial z}\right)^2\right], \tag{13a}$$

$$P_b = \frac{\mu_T}{\sigma_T}\frac{g}{\rho}\frac{\partial \rho}{\partial z}, \tag{13b}$$

$$\frac{\mu_{eff}}{\sigma_{eff}} = \frac{\mu}{\sigma} + \frac{\mu_T}{\sigma_T}, \tag{13c}$$

$$\mu_{eff} = C_\mu \rho \frac{k^2}{\varepsilon} + \rho \sigma_T v_T^d, \tag{13d}$$

$$v_T^d = \min(\alpha N^{-1}, v_o), \tag{13e}$$

where α, C_μ, $C_{1\varepsilon}$, $C_{2\varepsilon}$, and $C_{3\varepsilon}$ are empirical constants, N the buoyancy frequency, v_t^d the turbulent deep water eddy viscosity, v_o a constant value to avoid singularity in the buoyancy frequency, and $C_{\varepsilon 3}$ is -0.4 for stable stratification and equal to 1 for unstable stratification.

The boundary conditions for k and ε read:

$$k = \left[\frac{u_*^3}{C_\mu^{3/4}} + \frac{\max(B, 0)\kappa d_1}{C_\mu^{3/4}}\right]^{2/3}, \tag{14a}$$

$$\varepsilon = \frac{u_*^3}{\kappa d_1},$$ (14b)

$$u_*^2 = \frac{\tau_s}{\rho_o},$$ (14c)

$$B = \frac{g}{\rho_o}\left[\frac{\partial \rho}{\partial T}\frac{F_n}{\rho_o c_p} + \frac{\partial \rho}{\partial S}F_{\text{salt}}\right],$$ (14d)

where d_1 is the distance from the boundary to the centre of the near-boundary grid cell, κ von Karman's constant, u_* the friction velocity, τ_s the wind surface stress and B the buoyancy flux due to net heat (F_n) and salt (F_{salt}) fluxes. In the absence of momentum and buoyancy fluxes, minimum values of k and ε are applied. The constants are discussed in greater detail in Omstedt & Axell (2003).

Initial conditions

The initial temperature and salinity conditions for the EMB were taken from January 1958. The temperature and salinity were 16.6°C and 38.5 PSU respectively, from the surface to a depth of 150 m. Then temperature and salinity changed linearly to 14.1°C and 38.7 PSU respectively, at a depth of 600 m. From a depth of 600 m to the bottom, temperature and salinity were set to 14.1°C and 38.7 PSU respectively. The initial conditions for the turbulent model assumed only constant and small values for the turbulent kinetic energy and its dissipation rate.

Appendix A2. Heat flux components

The sensible heat flux F_h is given by

$$F_h = C_H \rho_a c_{pa} W_a (T_s - T_a), \tag{15}$$

where C_H is the heat transfer coefficient and c_{pa} the heat capacity of air. The latent heat flux F_e is calculated as

$$F_e = C_E \rho_a L_e W_a (q_s - q_a), \tag{16}$$

where q_s is the specific humidity of air at the sea surface, assumed to be equal to the saturation value at temperature T_s, calculated as

$$q_s = \frac{0.622 R_s}{P_a} \exp\left(\frac{c_{q1} T_s}{T_s + 273.15 - c_{q2}}\right), \tag{17}$$

where $R_s = 611$, $c_{q1} = 17.27$, $c_{q2} = 35.86$, and P_a is the air pressure at the reference level. The specific humidity of air at the reference level q_a is accordingly calculated as

$$q_a = \frac{0.622 R_s R_h}{P_a} \exp\left(\frac{c_{q1} T_a}{T_a + 273.15 - c_{q2}}\right), \tag{18}$$

where R_h is the relative humidity ($0 \leq R_h \leq 1$).

The heat flux due to net long-wave radiation F_l is given by the difference between the upward and downward propagation of long-wave radiation (Bodin 1979), according to:

$$F_l = \varepsilon_s \sigma_s (T_s + 273.15)^4 - \sigma_s (T_a + 273.15)^4 (a_1 + a_2 e_a^{1/2})(1 + a_3 N^2), \tag{19}$$

where ε_s is the emissivity of the sea surface, σ_s the Stefan-Boltzmann coefficient, and a_1, a_2 and $a_3 = 0.68$, 0.0036 and 0.18 are constants. Furthermore, N_c is the cloud coverage and e_a is the water vapour pressure in the atmosphere, related to q_a as follows:

$$e_a = \frac{P_a}{0.622} q_a. \tag{20}$$

The solar radiation to the water surface F_s is also calculated according to Bodin (1979):

$$F_s = \varepsilon_t S_0 \cos \Theta_a (f_t - f_a)(1 - f_c N_c), \tag{21}$$

where ε_t is the atmospheric turbidity, S_0 the solar constant, Θ_a the zenith angle, f_t and f_a the transmission and absorption functions respectively, and f_c a cloud function.

The short-wave radiation flux penetrating the open-water surface is given by

$$F_s^w = F_s (1 - \alpha_w), \tag{22}$$

where α_w is the surface-water albedo calculated from the Fresnel formulas (Jerlov 1968):

$$\alpha_w = \frac{1}{2}\left[\frac{\tan^2(\Theta_a - \Theta_w)}{\tan^2(\Theta_a + \Theta_w)} + \frac{\sin^2(\Theta_a - \Theta_w)}{\sin^2(\Theta_a + \Theta_w)}\right],\tag{23}$$

where Θ_a and Θ_w are the angles between the z-axis and the rays in the atmosphere and water respectively. Further details concerning the heat fluxes and constants are given in Omstedt & Axell (2003).